Ancient climate change, antifreeze, and the evolutionary diversification of Antarctic fishes

Thomas J. Near[a,b,1], Alex Dornburg[b], Kristen L. Kuhn[b], Joseph T. Eastman[c], Jillian N. Pennington[b,d], Tomaso Patarnello[e], Lorenzo Zane[f], Daniel A. Fernández[g], and Christopher D. Jones[h]

[a]Peabody Museum of Natural History and [b]Department of Ecology and Evolutionary Biology, Yale University, New Haven, CT 06520 [c]Department of Biomedical Sciences, College of Osteopathic Medicine, Ohio University, Athens, OH 45701; [d]Ezra Stiles College, Yale University, New Haven, CT 06520 [e]Department of Public Health, Comparative Pathology and Veterinary Hygiene, Università di Padova, 35020 Legnaro, Italy; [f]Department of Biology, Università di Padova, 35131 Padua, Italy; [g]Centro Austral de Investigaciones Científicas, 9410 Ushuaia, Argentina; and [h]Antarctic Ecosystem Research Division, Southwest Fisheries Science Center, National Oceanic and Atmospheric Administration National Marine Fisheries Service, La Jolla, CA 92037

Edited by David M. Hillis, University of Texas, Austin, TX, and approved January 25, 2012 (received for review September 15, 2011)

The Southern Ocean around Antarctica is among the most rapidly warming regions on Earth, but has experienced episodic climate change during the past 40 million years. It remains unclear how ancient periods of climate change have shaped Antarctic biodiversity. The origin of antifreeze glycoproteins (AFGPs) in Antarctic notothenioid fishes has become a classic example of how the evolution of a key innovation in response to climate change can drive adaptive radiation. By using a time-calibrated molecular phylogeny of notothenioids and reconstructed paleoclimate, we demonstrate that the origin of AFGP occurred between 42 and 22 Ma, which includes a period of global cooling approximately 35 Ma. However, the most species-rich lineages diversified and evolved significant ecological differences at least 10 million years after the origin of AFGPs, during a second cooling event in the Late Miocene (11.6–5.3 Ma). This pattern indicates that AFGP was not the sole trigger of the notothenioid adaptive radiation. Instead, the bulk of the species richness and ecological diversity originated during the Late Miocene and into the Early Pliocene, a time coincident with the origin of polar conditions and increased ice activity in the Southern Ocean. Our results challenge the current understanding of the evolution of Antarctic notothenioids suggesting that the ecological opportunity that underlies this adaptive radiation is not linked to a single trait, but rather to a combination of freeze avoidance offered by AFGPs and subsequent exploitation of new habitats and open niches created by increased glacial and ice sheet activity.

Notothenioidei | Icefish | Percomorpha | molecular clock | buoyancy

The recent onset of global climate change is causing an increase in temperatures for most regions of the Southern Ocean (1, 2), and is predicted to affect Antarctic marine species through increased physiological stress (3, 4), reduced ice scouring in near-shore habitats (5), and declining phytoplankton and krill populations that comprise the basis of Southern Ocean food webs (3, 6, 7). However, the effect of increasing ocean temperatures on Antarctic fishes is unknown. Teleost fishes are of fundamental importance to Southern Ocean ecology, providing the primary link between high-level vertebrate predators (e.g., toothed whales, penguins, and seals) and lower trophic levels (8). As the teleost fish diversity, abundance, and biomass of the Southern Ocean consists primarily of a single lineage of closely related species, the notothenioids (9), understanding how ancient climatic transitions between periods of global warming and cooling have influenced the patterns of diversification in these fishes is important to the development of forecasts on the impact of present-day climate change on Antarctic biodiversity.

Several characteristics suggest that the living diversity of Antarctic notothenioids was the result of adaptive radiation (10): they exhibit common ancestry (9) and a strong correlation between phenotype and habitat utilization (11, 12), they possess antifreeze glycoproteins (AFGPs) that allow them to occupy freezing habitats unavailable to most other teleosts (13), and they are more species-rich than their non-Antarctic sister lineage (approximately 100 vs. one species) (9). Molecular divergence time analyses have attempted to correlate the origin of the AFGP-bearing Antarctic notothenioids with a period of global cooling and widespread glaciation of Antarctica that began at the onset of the Eocene–Oligocene boundary (14, 15), approximately 35 Ma (16, 17), leading to the conclusion that the evolutionary innovation of AFGP was the trigger of the notothenioid adaptive radiation (15).

One critical aspect of the Antarctic notothenioid adaptive radiation that requires investigation is the relationship between paleoclimatic change and the tempo of lineage diversification. The AFGP innovation hypothesis predicts that the changing climatic conditions during the Oligocene cooling event, coupled with the evolution of AFGP, triggered increased rates of lineage and phenotypic diversification (15). This suggests that most of the ecological and phenotypic disparity observed among lineages of Antarctic notothenioids evolved early in their history. Subsequent climatic changes in the Southern Ocean, such as warming and glacial retreat during the Middle Miocene climatic optimum, dated between 17 and 14 Ma, or the Middle Miocene climatic transition (MMCT) that initiated the formation of subzero polar conditions between 14.2 and 13.8 Ma (18), will have had a secondary and less pronounced influence on the diversification of Antarctic notothenioids.

In addition to the origin of AFGP, the diversification of structural buoyancy adaptations in notothenioids is another critical component of this Antarctic adaptive radiation that reflects diversification along ecological axes (13) and a correlation between phenotype and habitat utilization (11). Although sharing a benthic common ancestor, Antarctic notothenioid species inhabit all parts of the water column in the Southern Ocean, spanning benthic to epibenthic, semipelagic, cryopelagic, and pelagic habitats (13). As all notothenioid species lack a swim bladder, buoyancy modification has been accomplished through the reduction of skeletal ossification, through alteration of the expression of collagen genes (19), and the evolution of extensive, and in some cases, unique lipid deposits (13, 20). Evolutionary analyses of teleost fish lineages often find a strong phylogenetic signal in ecomorphological traits (21, 22). Therefore, under the AFGP innovation model, disparity in buoyancy and lineage

Author contributions: T.J.N., A.D., J.T.E., T.P., L.Z., D.A.F., and C.D.J. designed research; T.J.N., A.D., K.L.K., J.T.E., J.N.P., and C.D.J. performed research; T.J.N., L.Z., and A.D. analyzed data; and T.J.N. and A.D. wrote the paper.

The authors declare no conflict of interest.

This article is a PNAS Direct Submission.

Data deposition: The sequences reported in this paper have been deposited in the GenBank database. For a list of accession numbers, see Table S1.

[1]To whom correspondence should be addressed. E-mail: thomas.near@yale.edu.

This article contains supporting information online at www.pnas.org/lookup/suppl/doi:10.1073/pnas.1115169109/-/DCSupplemental.

diversification should be intimately linked. This linkage is expected in a niche-filling model whereby lineage and character diversification occur early in a clade's history, and closely related species tend to be more similar in their traits and ecology (10, 23).

We investigated the tempo and mode of Antarctic notothenioid diversification through a set of comparative analyses that used a time-calibrated molecular phylogeny inferred from 83 notothenioid species (Table S1), and information on the paleoclimate of the Southern Ocean, the presence or absence of AFGP in notothenioid species, and field-collected measurements of buoyancy for more than 50 notothenioid species. The results of our analyses show that patterns of lineage and character diversification in notothenioids is more complex than the pattern expected from the conventional Oligocene-aged adaptive radiation scenario. We provide evidence that multiple constituent evolutionary radiations, coincident with more recent climate change events, more accurately characterize the evolutionary history of Antarctic notothenioids. Our results indicate that the evolution of AFGP predates the evolution of the exceptional morphological and ecological diversity in Antarctic notothenioids by at least 10 million years, and that the origin of this radiation is more closely correlated with climate change since the Late Miocene.

Results and Discussion

The use of Bayesian and maximum-likelihood methods resulted in strongly supported notothenioid molecular phylogenies (Fig. 1 and Fig. S1), and there was little difference between the phylogenies inferred from nuclear and mtDNA genes (Figs. S2 and S3). By using a Bayesian framework that relaxes the molecular clock (24), we obtained a mean posterior age estimate for the Antarctic clade at 22.4 Ma (Table S2), which corroborates estimates from previous studies (14, 15) and correlates with the Mi1 event (25), a time period of global cooling and ice sheet expansion in Antarctica. However, the mean posterior molecular age estimates for the most species-rich Antarctic notothenioid clades (e.g., *Trematomus*, 9.1 Ma; Channichthyidae, 6.3 Ma; and Artedidraconidae, 3.0 Ma) indicate most of the living diversity of notothenioids originated more than 10 million years after the origin of the Antarctic clade, coincident with the onset of

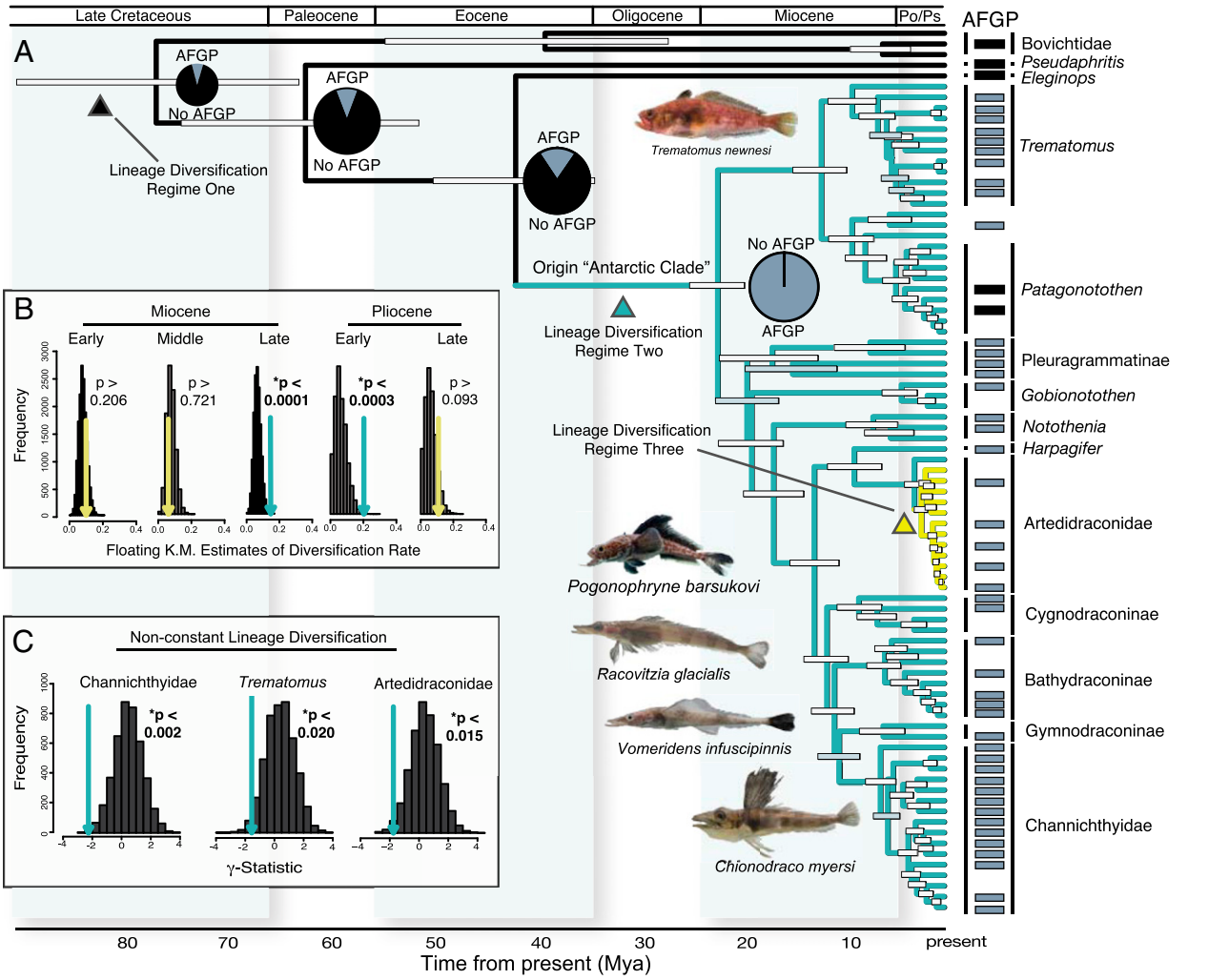

Fig. 1. Notothenioid chronogram with ancestral state reconstructions of AFGP and patterns of lineage diversification. (*A*) Bayesian inferred time tree of 83 notothenioid species. Bars at nodes represent 95% highest posterior density intervals of age estimates, with white bars showing posterior support 0.95 or greater. Branch colors and triangles correspond to the three best-fit lineage diversification regimes. Taxonomic classifications and presence (gray bar) or absence (black bar) of AFGP for notothenioid species are marked at the tips of the phylogeny. Posterior probabilities of Bayesian ancestral state reconstructions of AFGP origins are indicated by pie charts at key nodes in the notothenioid phylogeny. (*B*) Kendall–Moran (K.M.) estimates of lineage diversification contrasted with simulated distributions for specified geological time intervals. (*C*) The frequency distribution of simulated γ-values, with arrows marking the calculated γ-statistic for Channichthyidae, *Trematomus*, and Artedidraconidae.

intensified cooling in the Southern Ocean following the MMCT (Fig. 2). We examined the time-calibrated phylogeny for shifts in lineage diversification with a method that accounts for unsampled species and incrementally fits increasingly complex models of lineage diversification by using a stepwise information theoretic approach (26). Relative to the background diversification rate, our analyses identified three lineage diversification regimes that involve two shifts in lineage diversification rates, corresponding to the branches leading to the common ancestor of the Antarctic clade and to the common ancestor of Artedidraconidae exclusive of *Artedidraco skottsbergi* (Fig. 1 and Fig. S1).

The shift in rate of lineage diversification leading to the Antarctic clade is consistent with the expectations of the AFGP innovation diversification hypothesis; however, this model-fitting approach may mask exceptional pulses of cladogenesis in younger lineages nested in the Antarctic clade. We tested for pulses of diversification that correspond to particular intervals of geologic time from the origin of the Antarctic clade at the Oligocene–Early Miocene boundary through the Pliocene and found that, contrary to the expectations from an AFGP innovation model of notothenioid adaptive radiation, there is an elevated pulse of lineage diversification that corresponds to an interval spanning the Late Miocene through Early Pliocene, and no pulses of diversification from the Early Miocene through the Middle Miocene (Fig. 1*B*). This temporal pulse of diversification is corroborated by the observation that patterns of lineage diversification within the Antarctic clade are more accurately characterized by pulses of lineage diversification within several nested and younger subclades that originated in the Late Miocene or Early Pliocene, subsequent to the warming period of the Middle Miocene climatic optimum (Fig. 1*C* and Table S3).

Although AFGP is essential for survival of these fishes, the results of the ancestral reconstruction analyses (Fig. 1*A* and Table S4) imply that the pulses of lineage diversification observed within derived clades of Antarctic notothenioids (e.g., *Trematomus* and Channichthyidae) are decoupled from the evolutionary origin of AFGP, which minimally dates to the most recent common ancestor (MRCA) of the Antarctic clade (Fig. 1). These combined results do not support the hypothesis that the key innovation of AFGP was the sole driver of the diversification of Antarctic notothenioids. Instead, the origin of the exceptional diversity in this clade is correlated with more recent periods of global climate change, some 10 million years after the origin of Antarctic clade (Fig. 2). Given that notothenioids are poorly represented in the fossil record (9), it is plausible that unobserved extinction has eroded the signature of an early rapid radiation as inferred from the paucity of branching events between the Oligocene cooling event and the MMCT (Fig. 2). Regardless, the results of our analyses provide strong evidence that the bulk of the phylogenetic and ecological diversity of living Antarctic notothenioids originated subsequent to the MMCT.

To test predictions of the AFGP innovation adaptive radiation model on ecomorphological diversification, we used field-collected buoyancy measurements from 54 species comprising more than 1,300 specimens (Table S5) in a series of disparity through time analyses (23). The global patterns of subclade disparity in the Antarctic clade, Channichthyidae, and *Trematomus* all resulted in positive mean disparity indices that are indicative of repeated colonization of benthic, epibenthic, semipelagic, and pelagic habitats among closely related lineages (Fig. 3 *A*–*C*). The rapid lineage diversification within more derived Antarctic notothenioid subclades and the variation in buoyancy among closely related species are marked departures from adaptive radiation theory, which is typically characterized by a pronounced increase in rate of morphological and/or ecological disparity that decreases through time as niches are filled by diversifying lineages (23).

The unexpected pattern of adaptive radiation observed in Antarctic notothenioids may be explained by the appearance of the unique environmental and physical conditions of near-shore marine habitats in the Southern Ocean following the onset of widespread sea ice in the Late Miocene. Approximately 14 Ma ago, the MMCT created the polar conditions characteristic of contemporary Antarctica, intensifying the physical and thermal barriers that isolate the marine fauna of the Southern Ocean (18), initiating the repeated scouring of large sections of the

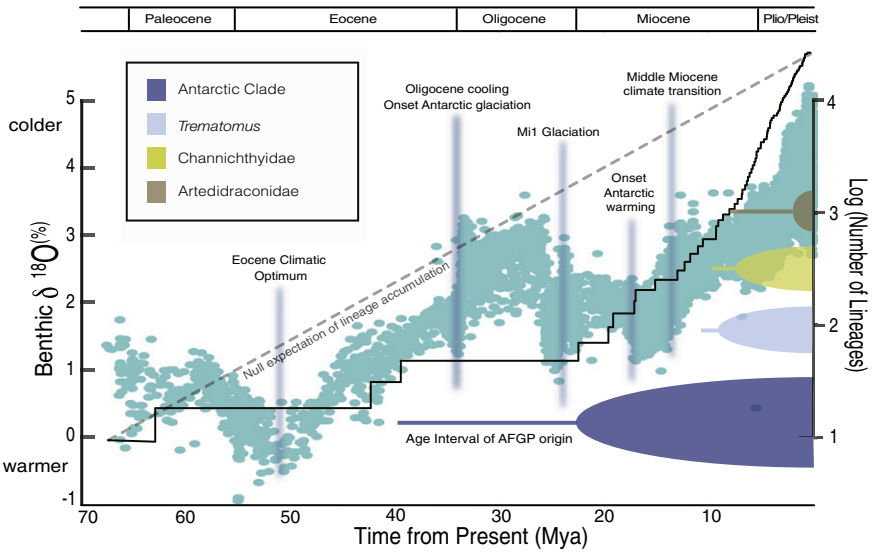

Fig. 2. Patterns of notothenioid lineage diversification and paleoclimate changes. Log-transformed accumulations of lineages through time are shown with a solid line. Expected pattern of lineage accumulations from a Yule pure-birth process is shown with a dashed line. Colored cones and lines match the crown and stem age estimates for the Antarctic clade, *Trematomus*, Channichthyidae, and Artedidraconidae. The interval reconstructed as the most probable evolutionary origin of AFGP is highlighted on the line depicting the stem phylogenetic lineage of the Antarctic clade. Blue filled circles represent oxygen isotope data for specific time periods taken with increased δ-^{18}O values corresponding to cooler climatic conditions (7). Major global paleoclimatic events since the Paleocene are highlighted with vertical blue-gray bars.

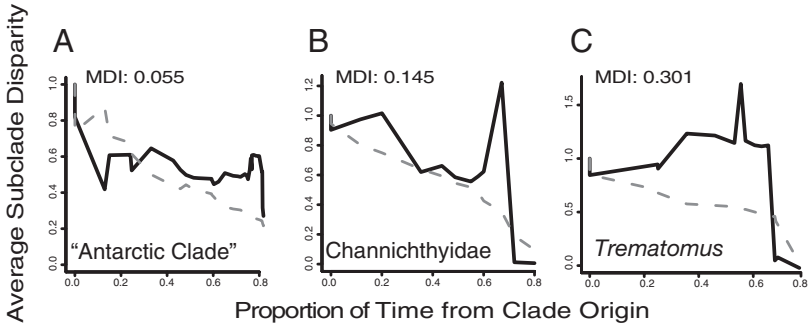

Fig. 3. Patterns of buoyancy disparity through time. Disparity in buoyancy through time is contrasted with simulations for (*A*) the entire Antarctic clade, (*B*) Channichthyidae, and (*C*) *Trematomus*. Mean disparity index (MDI) values were calculated omitting the most recent 20% of the chronogram. Solid lines are the observed patterns of buoyancy disparity, and dotted lines are the median value of the Brownian motion simulations.

continental shelf by glaciers, icebergs (27), and sometimes ice sheets advancing as far as the shelf break (28). This ice activity resulted in periodic extinction of the near-shore benthic fauna (29), allowing for subsequent colonization of previously occupied niche space, as well as creating opportunities for geographic isolation and speciation. The ecological opportunities resulting from repeated creation of open niches through extinction of potential competitors, over substantial expanses of geologic time, could result in the evolution of the unusual pattern of substantial morphological and ecological disparity within Antarctic notothenioid subclades.

Our results highlight the dependence of the primary component of the contemporary Antarctic fish fauna on ecological opportunity associated with historical global climate change and the persistence of subzero polar conditions. We find that the origin of AFGP, despite its being essential for survival in subzero marine habitats, did not alone drive the exceptional diversity of extant Antarctic notothenioids. In contrast, this major component of the Southern Ocean's marine biota has been shaped through evolutionary time by a combination of freeze avoidance offered by AFGP, and abiotic factors initiated by paleoclimatic changes that resulted in continuous ecological divergence into recurrently opening niches. In a tragic twist of fate, the development of polar climatic conditions that shaped the radiation of Antarctic notothenioids is now reversing, and the increasing temperature of the Southern Ocean (1), with the associated potential for the arrival of invasive species and disruption of food webs (3, 6, 30), is the greatest threat to the survival of this unparalleled radiation of teleosts.

Materials and Methods

Phylogenetic Data and Analyses. Standard phenol-chloroform extraction protocol or Qiagen DNeasy Blood and Tissue kits were used to isolate DNA from tissue biopsies sampled from 83 notothenioid species (Table S1). Previously published PCR primers were used to amplify and sequence two mtDNA genes (*nd2* and *16S* rRNA) and five nuclear gene regions (*RPS71*, *myh6*, *sh3px3*, *tbr1*, and *zic1*) that consisted of four unlinked exons and a single intron (31–34). Protein coding gene regions (*nd2*, *myh6*, *sh3px3*, *tbr1*, and *zic1*) were aligned by using the computer program MUSCLE (35) and refined by eye using the inferred amino acid sequences. No frame mutations or DNA substitutions that resulted in stop codons were observed in the aligned sequences. The noncoding genes (*RPS71* and *16S* rRNA) were aligned by using the computer program MUSCLE. The combined seven-gene dataset contained 6,431 bp, and 98.9% of data matrix (taxa and genes) was complete.

Nine data partitions were designated that corresponded to the three separate codon positions for the mtDNA protein coding gene, a single partition for the mtDNA 16S rRNA, and a single partition for each of the five nuclear genes. Potential partitioning strategies included a single partition for each protein coding gene vs. three codon positions in each of these genes and were assessed by using Bayes factor comparisons of the posterior harmonic mean of the maximum likelihood score from Bayesian phylogenetic analyses. A GTR+G substitution model was used in a partitioned maximum likelihood analysis by using the computer program RAxML 7.2.6 (36) run with the –D option. Support for nodes in the RAxML inferred tree was assessed by using a thorough bootstrap analysis (option –f i) with 2,000 replicates.

Relaxed Molecular Clock Analyses. Divergence times of notothenioids were estimated by using an uncorrelated lognormal (UCLN) model of molecular evolutionary rate heterogeneity implemented in the computer program BEAST version 1.6.1 (24, 37). The seven-gene dataset was partitioned as in the maximum likelihood phylogenetic analysis described earlier, unlinking the UCLN clock and nucleotide substitution models across partitions. Based on the results of a previous UCLN analysis (15), age priors with a normal distribution were applied to four nodes in the notothenioid phylogeny, which included the MRCA of all notothenioids (mean, 71.4; SD, 11.0), the MRCA of *Pseudaphritis urvillii* and all other notothenioids (mean, 63.0; SD, 10.4), the MRCA of *Eleginops maclovinus* and the Antarctic clade (mean, 42.9; SD, 8.0), and the MRCA of the Antarctic clade (mean, 23.8; SD, 1.5). A birth–death speciation prior was used for branching rates in the phylogeny. The BEAST analyses were run five times with each run consisting of 3.0×10^7 generations, sampling at every 1,000 generations. The resulting trees and log files from each of the five runs were combined by using the computer program LogCombiner version 1.6.1 (http://beast.bio.ed.ac.uk/LogCombiner). Convergence of model parameter values and estimated node heights to their optimal posterior distributions was assessed by plotting the marginal posterior probabilities versus the generation state in the computer program Tracer version 1.5 (http://beast.bio.ed.ac.uk/Tracer). Effective sample size values were calculated for each parameter to ensure adequate mixing of the Markov Chain Monte Carlo (MCMC; effective sample size > 200). The posterior probability density of the combined tree and log files was summarized as a maximum clade credibility tree using TreeAnnotator version 1.6.1 (http://beast.bio.ed.ac.uk/TreeAnnotator).

Assessing Patterns of Lineage Diversification. Diversification rate analyses of notothenioids were performed by using the APE (38), GEIGER (39), and LASER (40, 41) software packages in R. Patterns of lineage accumulation through time were visualized by using a lineage-through-time plot (42). To determine if any notothenioid subclades exhibit departures from a global background rate of lineage diversification, we used MEDUSA, a step-wise Akaike Information Criterion (AIC) approach that incrementally fits increasingly complex models of lineage diversification to a time calibrated phylogeny (26). This method initially calculates the AIC fit of a two-parameter birth–death model of cladogenesis to the time-calibrated phylogeny and compares this score with the AIC score of a more complex five-parameter model in which two birth rates, two death rates, and an optimal shift point on the phylogeny is estimated. By using an AIC threshold of four to denote a substantial improvement in model fit by the more complex model (43), the step-wise function repeats this model selection process by retaining the more complex parameter rich model and comparing its fit to a model that includes an additional birth, death, and shift-point parameter. This iterative model-building process continues until the addition of new parameters no longer offers an improvement in AIC score. To account for the influence of incomplete taxon sampling on the birth, death, and shift-point parameter estimates, MEDUSA employs a "diversity tree" as its framework. Briefly, a diversity tree is constructed by collapsing lineages with missing taxa and assigning a species richness value to these resulting stem lineages. For clades with complete taxon sampling, tip taxa are not pruned, and

instead assigned a diversity of one (44). Because we sampled more than 75% of the notothenioid species diversity, we assigned most taxa a species richness value of one. Following a list of notothenioid species (45), we collapsed *Harpagifer* to include six species, *Pleuragramma* plus *Aethotaxis* to include three species to account for not sampling *Gvozdarus svetovidovi*, *Notothenia* to include five species as *Notothenia microlepidota* and *Paranotothenia magellanica* were not sampled, *Patagonotothen* to include 14 species, *Psilodraco* to include two species to reflect the lack of *Acanthodraco dewitti* from our analysis, *Bovichtus* to include nine species, and *Trematomus newnesi* to include two species to account for not sampling *Cryothenia*.

To determine if lineage diversification dynamics within notothenioids are best modeled by a single shift point in rates or if inferred shifts in diversification rates were driven by pulses of cladogenesis corresponding to specific time intervals, we calculated floating-point Kendall–Moran estimates of diversification rate for each subdivision of the Miocene and Pliocene, and the Late Miocene and Early Pliocene combined (46). Time interval-specific diversification rate estimates were compared with null distributions generated by simulating 10,000 birth–death trees by using maximum-likelihood values of speciation and extinction. Simulated phylogenies were generated to capture the extant taxonomic diversity of notothenioids, and then resampled to reflect the taxon sampling in the molecular time-calibrated phylogenies.

We investigated if lineage diversification in the major species-rich Antarctic notothenioid subclades was constant over time by assessing the significance of the γ-statistic by using the Monte Carlo constant rates test (MCCR) (47). We compared observed values of γ to a null distribution of 10,000 pure-birth trees simulated under the global estimates of speciation (λ_G) and extinction (μ_G) that were calculated using a method of moments estimator (48). As the MCCR test is prone to high type I error rates if the initial taxon sampling strategy was nonrandom (49), we repeated all MCCR analyses by using the proportionately older splits simulation protocol that assumes that nonsampled lineages are more likely to be younger (50). All MCCR tests were repeated to incorporate the credible range of maximum likelihood estimates of λ_G and μ_G.

Estimation of AFGP Ancestral States. We compiled a dataset from the literature on the presence (scored as 1) and absence (scored as 0) of AFGP for 47 notothenioid species (Fig. 1 and Table S4) based on genomic Southern blots (51, 52), freezing-point depression of body fluids (53–55), or isolation of the AFGP (56). Species for which there is no information on the presence of AFGP were pruned from the posterior set of Bayesian-inferred time-calibrated phylogenies (Fig. 1). Ancestral character states for AFGP were estimated by using the modified posterior distribution of trees in the computer program BayesTraits that incorporates a reversible-jump MCMC (RJ-MCMC) with an exponential hyperprior on the rate coefficients to integrate over the uncertainty present in the fit of models of character evolution to the data (57, 58). We ran five replicate sets of BayesTraits analyses with the RJ-MCMC sampling for 200 million generations, sampling every 2,000 and discarding the first 25% of the runs as burn-in. Log files were processed by using custom-written scripts in R to visualize the posterior distribution of the RJ-MCMC–inferred ancestral reconstructions of AFGP presence or absence.

Patterns of Disparity in Buoyancy. Field captured specimens were heavily anesthetized with tricaine methanesulfonate and weighed in seawater at ambient temperatures and weighed in air (11). Buoyancy (%B) was expressed as the percentage of the weight in air (W_{Air}) supported in water (W_{Water}) as follows (Table S5):

$$\%B = W_{Water}/W_{Air} \times 10^2 \quad [1]$$

Most buoyancy measurements were made during Southern Ocean expeditions in 2001, 2003, 2004, 2006, and 2009; however, some were presented in earlier publications (11, 59, 60). We tested the hypothesis that notothenioid lineages have partitioned more disparity in buoyancy between, rather than within, subclades by calculating the average relative subclade disparity through time of the buoyancy data for the notothenioid Antarctic clade and the major Antarctic subclades (23). In each disparity-through-time analysis, we assessed whether the observed morphological disparity index (MDI) differed from a null model of Brownian evolution by calculating the empirical variance and simulating the evolution of buoyancy on the time-calibrated notothenioid phylogeny 1,000 times by using the Geiger package of computer programs for R (39). Negative MDI values indicate that more morphological disparity is distributed between subclades whereas positive values indicate that subclades have converged on a pattern whereby overall morphological disparity is partitioned among members within each subclade. As incomplete sampling can influence the calculation of the MDI, we restricted our analysis of MDI values to the first 80% of the time-calibrated phylogeny.

ACKNOWLEDGMENTS. We thank A. L. DeVries and C.-H. C. Cheng for supporting our initial studies of Antarctic fishes. Field and laboratory support was provided by H. W. Detrich, J. Kendrick, K.-H. Kock, J. A. Moore, and A. L. Stewart. A. L. DeVries and C.-H. C. Cheng (University of Illinois), G. Lecointre (Muséum National d'Histoire Naturelle, Paris, France), and C. D. Roberts (Museum of New Zealand Te Papa Tongarewa) provided critical specimens. K. L. Prudic, M. E. Alfaro, J. M. Beaulieu, M. J. Donoghue, R. I. Eytan, A. M. Near, and J. C. Oliver provided comments on previous versions of this manuscript. Fieldwork was facilitated through the United States Antarctic Marine Living Resources Program and the officers and crew of the RV *Yuzhmorgeologiya*, and the 2004 ICEFISH cruise aboard the *RVIB Nathaniel B. Palmer*, which was funded through National Science Foundation (NSF) Grant OPP 01-32032 (to H. William Detrich III). This research was supported by NSF Grants ANT-0839007 (to T.J.N.), DEB-0716155 (to T.J.N.), DEB-1061806 (to T.J.N.), and ANT-0436190 (to J.T.E.).

1. Gille ST (2002) Warming of the Southern Ocean since the 1950s. *Science* 295: 1275–1277.
2. Turner J, Lachlan-Cope TA, Colwell S, Marshall GJ, Connolley WM (2006) Significant warming of the Antarctic winter troposphere. *Science* 311:1914–1917.
3. Barnes DKA, Peck LS (2008) Vulnerability of Antarctic shelf biodiversity to predicted regional warming. *Clim Res* 37:149–163.
4. Somero GN (2010) The physiology of climate change: How potentials for acclimatization and genetic adaptation will determine 'winners' and 'losers'. *J Exp Biol* 213: 912–920.
5. Smale DA, Brown KM, Barnes DKA, Fraser KPP, Clarke A (2008) Ice scour disturbance in Antarctic waters. *Science* 321:371–371.
6. Atkinson A, Siegel V, Pakhomov E, Rothery P (2004) Long-term decline in krill stock and increase in salps within the Southern Ocean. *Nature* 432:100–103.
7. Trivelpiece WZ, et al. (2011) Variability in krill biomass links harvesting and climate warming to penguin population changes in Antarctica. *Proc Natl Acad Sci USA* 108: 7625–7628.
8. La Mesa M, Eastman JT, Vacchi M (2004) The role of notothenioid fish in the food web of the Ross Sea shelf waters: A review. *Polar Biol* 27:321–338.
9. Eastman JT (2005) The nature of the diversity of Antarctic fishes. *Polar Biol* 28:93–107.
10. Schluter D (2000) *The Ecology of Adaptive Radiation* (Oxford Univ Press, Oxford).
11. Eastman JT, DeVries AL (1982) Buoyancy studies of notothenioid fishes in McMurdo Sound, Antarctica. *Copeia* 1982:385–393.
12. Rutschmann S, et al. (2011) Parallel ecological diversification in Antarctic notothenioid fishes as evidence for adaptive radiation. *Mol Ecol* 20:4707–4721.
13. Eastman JT (1993) *Antarctic Fish Biology: Evolution in a Unique Environment* (Academic, San Diego).
14. Near TJ (2004) Estimating divergence times of notothenioid fishes using a fossil-calibrated molecular clock. *Antarct Sci* 16:37–44.
15. Matschiner M, Hanel R, Salzburger W (2011) On the origin and trigger of the notothenioid adaptive radiation. *PLoS ONE* 6:e18911.
16. Zachos J, Pagani M, Sloan L, Thomas E, Billups K (2001) Trends, rhythms, and aberrations in global climate 65 Ma to present. *Science* 292:686–693.
17. DeConto RM, Pollard D (2003) Rapid Cenozoic glaciation of Antarctica induced by declining atmospheric CO2. *Nature* 421:245–249.
18. Shevenell AE, Kennett JP, Lea DW (2004) Middle Miocene Southern Ocean cooling and Antarctic cryosphere expansion. *Science* 305:1766–1770.
19. Albertson RC, et al. (2010) Molecular pedomorphism underlies craniofacial skeletal evolution in Antarctic notothenioid fishes. *BMC Evol Biol* 10:10.
20. DeVries AL, Eastman JT (1978) Lipid sacs as a buoyancy adaptation in an Antarctic fish. *Nature* 271:352–353.
21. Price SA, Holzman R, Near TJ, Wainwright PC (2011) Coral reefs promote the evolution of morphological diversity and ecological novelty in labrid fishes. *Ecol Lett* 14: 462–469.
22. Sidlauskas B (2008) Continuous and arrested morphological diversification in sister clades of characiform fishes: A phylomorphospace approach. *Evolution* 62:3135–3156.
23. Harmon LJ, Schulte, JA, II, Larson A, Losos JB (2003) Tempo and mode of evolutionary radiation in iguanian lizards. *Science* 301:961–964.
24. Drummond AJ, Ho SYW, Phillips MJ, Rambaut A (2006) Relaxed phylogenetics and dating with confidence. *PLoS Biol* 4:e88.
25. Naish TR, et al. (2001) Orbitally induced oscillations in the East Antarctic ice sheet at the Oligocene/Miocene boundary. *Nature* 413:719–723.
26. Alfaro ME, et al. (2009) Nine exceptional radiations plus high turnover explain species diversity in jawed vertebrates. *Proc Natl Acad Sci USA* 106:13410–13414.
27. Tripati AK, Roberts CD, Eagle RA (2009) Coupling of CO2 and ice sheet stability over major climate transitions of the last 20 million years. *Science* 326:1394–1397.
28. Pollard D, DeConto RM (2009) Modelling West Antarctic ice sheet growth and collapse through the past five million years. *Nature* 458:329–332.
29. Thatje S, Hillenbrand CD, Mackensen A, Larter R (2008) Life hung by a thread: Endurance of Antarctic fauna in glacial periods. *Ecology* 89:682–692.

30. Schofield O, et al. (2010) How do polar marine ecosystems respond to rapid climate change? *Science* 328:1520–1523.
31. Kocher TD, Conroy JA, McKaye KR, Stauffer JR, Lockwood SF (1995) Evolution of NADH dehydrogenase subunit 2 in east African cichlid fish. *Mol Phylogenet Evol* 4: 420–432.
32. Near TJ, Pesavento JJ, Cheng CHC (2004) Phylogenetic investigations of Antarctic notothenioid fishes (Perciformes: Notothenioidei) using complete gene sequences of the mitochondrial encoded 16S rRNA. *Mol Phylogenet Evol* 32:881–891.
33. Li CH, Ortí G, Zhang G, Lu GQ (2007) A practical approach to phylogenomics: The phylogeny of ray-finned fish (Actinopterygii) as a case study. *BMC Evol Biol* 7:44.
34. Chow S, Hazama K (1998) Universal PCR primers for S7 ribosomal protein gene introns in fish. *Mol Ecol* 7:1255–1256.
35. Edgar RC (2004) MUSCLE: Multiple sequence alignment with high accuracy and high throughput. *Nucleic Acids Res* 32:1792–1797.
36. Stamatakis A (2006) RAxML-VI-HPC: Maximum likelihood-based phylogenetic analyses with thousands of taxa and mixed models. *Bioinformatics* 22:2688–2690.
37. Drummond AJ, Rambaut A (2007) BEAST: Bayesian evolutionary analysis by sampling trees. *BMC Evol Biol* 7:214.
38. Paradis E, Claude J, Strimmer K (2004) APE: Analyses of phylogenetics and evolution in R language. *Bioinformatics* 20:289–290.
39. Harmon LJ, Weir JT, Brock CD, Glor RE, Challenger W (2008) GEIGER: Investigating evolutionary radiations. *Bioinformatics* 24:129–131.
40. Rabosky DL (2006) Likelihood methods for detecting temporal shifts in diversification rates. *Evolution* 60:1152–1164.
41. Rabosky DL (2006) LASER: A maximum likelihood toolkit for detecting temporal shifts in diversification rates from molecular phylogenies. *Evol Bioinform Online* 2:273–276.
42. Nee S, Mooers AO, Harvey PH (1992) Tempo and mode of evolution revealed from molecular phylogenies. *Proc Natl Acad Sci USA* 89:8322–8326.
43. Burnham KP, Anderson DR (2004) Multimodel inference: Understanding AIC and BIC in model selection. *Sociol Methods Res* 33:261–304.
44. Slater GJ, Price SA, Santini F, Alfaro ME (2010) Diversity versus disparity and the radiation of modern cetaceans. *Proc Biol Sci* 277:3097–3104.
45. Eastman JT, Eakin RR (2000) An updated species list of notothenioid fish (Perciformes; Notothenioidei), with comments on Antarctic species. *Arch Fisch Meeresforsch* 48:11–20.
46. Dornburg A, Santini F, Alfaro ME (2008) The influence of model averaging on clade posteriors: An example using the triggerfishes (Family Balistidae). *Syst Biol* 57: 905–919.
47. Pybus OG, Harvey PH (2000) Testing macro-evolutionary models using incomplete molecular phylogenies. *Proc Biol Sci* 267:2267–2272.
48. Magallón S, Sanderson MJ (2001) Absolute diversification rates in angiosperm clades. *Evolution* 55:1762–1780.
49. Fordyce JA (2010) Interpreting the gamma statistic in phylogenetic diversification rate studies: A rate decrease does not necessarily indicate an early burst. *PLoS ONE* 5: e11781.
50. Brock CD, Harmon LJ, Alfaro ME (2011) Testing for temporal variation in diversification rates when sampling is incomplete and nonrandom. *Syst Biol* 60: 410–419.
51. Cheng C-HC, Chen LB, Near TJ, Jin YM (2003) Functional antifreeze glycoprotein genes in temperate-water New Zealand nototheniid fish infer an Antarctic evolutionary origin. *Mol Biol Evol* 20:1897–1908.
52. Cheng C-HC, Detrich, HW, 3rd (2007) Molecular ecophysiology of Antarctic notothenioid fishes. *Philos Trans R Soc Lond B Biol Sci* 362:2215–2232.
53. DeVries AL, Wohlschlag DE (1969) Freezing resistance in some Antarctic fishes. *Science* 163:1073–1075.
54. DeVries AL (1971) Glycoproteins as biological antifreeze agents in antarctic fishes. *Science* 172:1152–1155.
55. DeVries AL, Lin Y (1977) *Adaptations Within Antarctic Ecosystems*, ed Llano GA (Smithsonian Institution, Washington, DC), pp 439–458.
56. Wohrmann APA (1996) Antifreeze glycopeptides and peptides in Antarctic fish species from the Weddell Sea and the Lazarev Sea. *Mar Ecol Prog Ser* 130:47–59.
57. Pagel M, Meade A, Barker D (2004) Bayesian estimation of ancestral character states on phylogenies. *Syst Biol* 53:673–684.
58. Pagel M, Meade A (2006) Bayesian analysis of correlated evolution of discrete characters by reversible-jump Markov chain Monte Carlo. *Am Nat* 167:808–825.
59. Near TJ, Kendrick BJ, Detrich HW, Jones CD (2007) Confirmation of neutral buoyancy in *Aethotaxis mitopteryx* DeWitt (Notothenioidei: Nototheniidae). *Polar Biol* 30: 443–447.
60. Fernández DA, Ceballos SG, Malanga G, Boy CC, Vanella FA (2012) Buoyancy of sub-Antarctic notothenioids including the sister lineage of all other notothenioids (Bovichthidae). *Polar Biol* 35:99–106.

Supporting Information

Near et al. 10.1073/pnas.1115169109

Fig. S1. Maximum likelihood phylogeny of 83 notothenioid species based on combined nuclear and mitochondrial DNA genes. The phylogeny was inferred from a nucleotide dataset consisting of two mitochondrial and five nuclear genes. Branch lengths are scaled to the estimated number of nucleotide substitutions. Filled circles at nodes within mark clades supported with a bootstrap score (2,000 replicates) equal to 100, and open circles mark clades supported with bootstrap scores ranging between 75 and 99.

Fig. S2. Maximum likelihood phylogeny of 83 notothenioid species based on DNA sequences from five nuclear genes. Branch lengths are scaled to the estimated number of nucleotide substitutions. Filled circles at nodes within mark clades supported with a bootstrap score (2,000 replicates) equal to 100, and open circles mark clades supported with bootstrap scores ranging between 75 and 99.

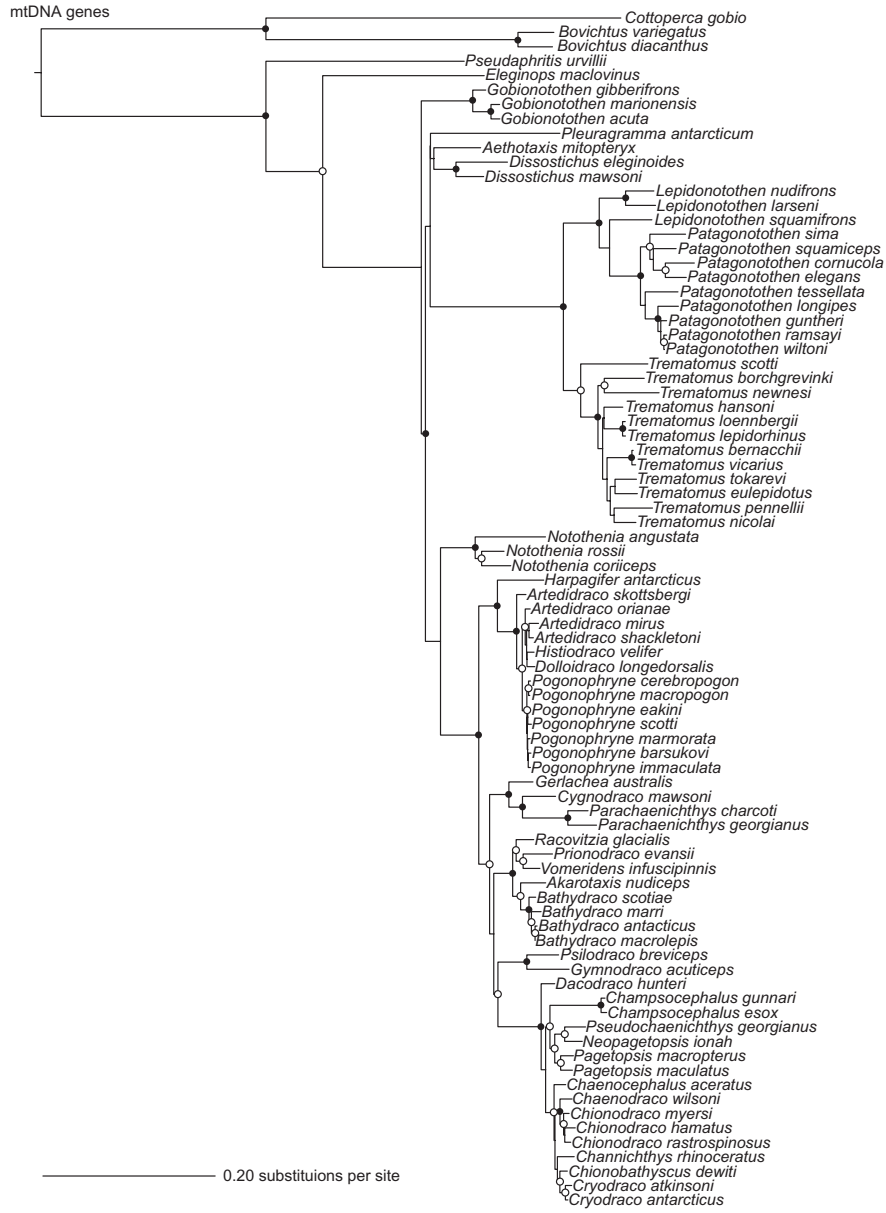

Fig. S3. Maximum likelihood phylogeny of 83 notothenioid species based on DNA sequences from two mitochondrial genes. Branch lengths are scaled to the estimated number of nucleotide substitutions. Filled circles at nodes within mark clades supported with a bootstrap score (2,000 replicates) equal to 100 and open circles mark clades supported with bootstrap scores ranging between 75 and 99.

Other Supporting Information Files

Table S1 (DOC)
Table S2 (DOC)
Table S3 (DOC)
Table S4 (DOC)
Table S5 (DOC)

Table S1. Species Sampled and GenBank Accession Numbers.

Species	**Family**	**Tissue Catalogue Number**	***nd2* GenBank**	***16S* rRNA GenBank**	***S7* intron 1 GenBank**	***myh6* Genbank**	***SH3PX3* Genbank**	***tbr1* Genbank**	***zic1* Genbank**
Bovichtus variegatus	Bovichtidae	YFTC 1721	JN186882	AY520101	JN186842	JN187019	JN186937	JN186978	JN186801
Bovichtus diacanthus	Bovichtidae	YFTC 3478	JN186883	JN186914	JN186843	JN187020	JN186938	JN186979	JN186802
Cottoperca gobio	Bovichtidae	YFTC 2301	JN186884	AY520102	JN186844	JN187021	JN186939	JN186980	JN186803
Pseudaphritis urvillii	Pseudaphritidae	YFTC 1463	JN186885	AY520104	JN186845	JN187022	JN186940	JN186981	JN186804
Eleginops maclovinus	Eleginopidae	YFTC 3993	JN186886	JN186915	JN186846	JN187023	JN186941	JN186982	JN186805
Dolloidraco longedorsalis	Artedidraconidae	YFTC 12894	FJ647587	HQ170297	FJ647619	HQ169792	HQ170179	HQ170238	HQ169672
Artedidraco mirus	Artedidraconidae	YFTC 2342	JN186887	JN186916	JN186847	JN187024	JN186942	JN186983	JN186806
Artedidraco orianae	Artedidraconidae	YFTC 4133	JN186888	JN186917	JN186848	JN187025	JN186943	JN186984	JN186807
Artedidraco shackletoni	Artedidraconidae	YFTC 4129	JN186889	JN186918	JN186849	JN187026	JN186944	JN186985	JN186808
Artedidraco skottsbergi	Artedidraconidae	YFTC 2295	FJ973333	JN186919	JN186850	JN187027	JN186945	JN186986	JN186809

Histiodraco velifer	Artedidraconidae	YFTC 2049	FJ973335	JN186920	JN186851	JN187028	JN186946	JN186987	JN186810
Pogonophryne barsukovi	Artedidraconidae	YFTC 7843	FJ973337	JN186921	JN186852	JN187029	JN186947	JN186988	JN186811
Pogonophryne cerebropogon	Artedidraconidae	YFTC 1797	JN186890	JN186922	JN186853	JN187030	JN186948	JN186989	JN186812
Pogonophryne eakini	Artedidraconidae	YFTC 9886	FJ973342	N/A	JN186854	JN187031	JN186949	JN186990	JN186813
Pogonophryne macropogon	Artedidraconidae	YFTC 9882	JN186891	JN186923	JN186855	JN187032	JN186950	JN186991	JN186814
Pogonophryne immaculata	Artedidraconidae	YFTC 13847	FJ973344	JN186924	JN186856	JN187033	JN186951	JN186992	JN186815
Pogonophryne marmorata	Artedidraconidae	YFTC 2023	FJ973350	JN186925	JN186857	JN187034	JN186952	JN186993	JN186816
Pogonophryne scotti	Artedidraconidae	YFTC 7672	JN186892	JN186926	JN186858	JN187035	JN186953	JN186994	JN186817
Akarotaxis nudiceps	Bathydraconidae	YFTC 12874	HQ170108	HQ170316	HQ170152	HQ169824	HQ170211	HQ170270	HQ169704
Bathydraco macrolepis	Bathydraconidae	YFTC 13895	HQ170110	HQ170318	HQ170154	HQ169826	HQ170213	HQ170272	HQ169706
Bathydraco marri	Bathydraconidae	YFTC 13884	HQ170111	HQ170319	HQ170156	HQ169828	HQ170215	HQ170274	HQ169708
Bathydraco antarcticus	Bathydraconidae	YFTC 13912	HQ170113	HQ170321	JN186859	HQ169830	HQ170217	HQ170276	HQ169710
Bathydraco scotiae	Bathydraconidae	YFTC 13892	HQ170115	HQ170323	HQ170159	HQ169832	HQ170219	HQ170278	HQ169712
Cygnodraco mawsoni	Bathydraconidae	YFTC 2050	HQ170116	HQ170324	HQ170160	HQ169833	HQ170220	HQ170279	HQ169713

Gerlachea australis	Bathydraconidae	YFTC 4417	HQ170118	HQ170326	HQ170162	HQ169835	HQ170222	HQ170281	HQ169715
Gymnodraco acuticeps	Bathydraconidae	YFTC 12080	HQ170120	HQ170328	HQ170165	HQ169838	HQ170225	HQ170284	HQ169718
Parachaenichthys charcoti	Bathydraconidae	YFTC 4494	HQ170122	HQ170330	HQ170167	HQ169840	HQ170227	HQ170286	HQ169720
Parachaenichthys georgianus	Bathydraconidae	YFTC 3946	HQ170123	HQ170331	HQ170168	HQ169841	HQ170228	HQ170287	HQ169721
Prionodraco evansii	Bathydraconidae	YFTC 2300	HQ170125	AY520137	HQ170170	HQ169843	HQ170230	HQ170289	HQ169723
Psilodraco breviceps	Bathydraconidae	YFTC 11037	HQ170128	HQ170336	HQ170173	HQ169846	HQ170233	HQ170292	HQ169726
Racovitzia glacialis	Bathydraconidae	YFTC 4449	HQ170130	HQ170337	HQ170174	HQ169848	HQ170235	HQ170294	HQ169728
Vomeridens infuscipinnis	Bathydraconidae	YFTC 20970	JN186893	N/A	JN186860	JN187036	JN186954	JN186995	JN186818
Chaenocephalus aceratus	Channichthyidae	YFTC 2002	AY249493	AY249466	HM166091	HQ169793	HQ170180	HQ170239	HQ169673
Chaenodraco wilsoni	Channichthyidae	YFTC 2003	AY249504	AY249477	HM165755	HQ169795	HQ170182	HQ170241	HQ169675
Champsocephalus esox	Channichthyidae	YFTC 3923	HQ170095	HQ170299	HQ170135	HQ169797	HQ170184	HQ170243	HQ169677
Champsocephalus gunnari	Channichthyidae	YFTC 2005	HQ170097	HQ170301	HQ170137	HQ169799	HQ170186	HQ170245	HQ169679
Channichthys rhinoceratus	Channichthyidae	YFTC 1987	AY249503	AY249476	HQ170139	HQ169801	HQ170188	HQ170247	HQ169681
Chionobathyscus dewitti	Channichthyidae	YFTC 4312	HQ170099	HQ170303	HQ170140	HQ169802	HQ170189	HQ170248	HQ169682

Chionodraco hamatus	Channichthyidae	YFTC 13772	HQ170101	HQ170305	HQ170142	HQ169804	HQ170191	HQ170250	HQ169684
Chionodraco myersi	Channichthyidae	YFTC 2044	HQ170103	HQ170307	HQ170145	HQ169807	HQ170194	HQ170253	HQ169687
Chionodraco rastrospinosus	Channichthyidae	YFTC 2006	AY249502	AY249475	HM165855	HQ169808	HQ170195	HQ170254	HQ169688
Cryodraco antarcticus	Channichthyidae	YFTC 2007	AY249494	AY249467	HM165959	HQ169810	HQ170197	HQ170256	HQ169690
Cryodraco atkinsoni	Channichthyidae	YFTC 2046	HQ170104	HQ170310	HQ170146	HQ169812	HQ170199	HQ170258	HQ169692
Dacodraco hunteri	Channichthyidae	YFTC 1988	AY249507	AY249479	HQ170148	HQ169814	HQ170201	HQ170260	HQ169694
Neopagetopsis ionah	Channichthyidae	YFTC 11038	HM165731	HQ170313	HM165690	HQ169817	HQ170204	HQ170263	HQ169697
Pagetopsis macropterus	Channichthyidae	YFTC 2011	AY249511	AY249484	HM165520	HQ169818	HQ170205	HQ170264	HQ169698
Pagetopsis maculatus	Channichthyidae	YFTC 2041	AY249512	AY249485	HQ170150	HQ169820	HQ170207	HQ170266	HQ169700
Pseudochaenichthys georgianus	Channichthyidae	YFTC 2010	AY249510	AY249483	HM165578	HQ169823	HQ170210	HQ170269	HQ169703
Harpagifer antarcticus	Harpagiferidae	YFTC 1731	JN186894	AY520130	JN186861	JN187037	JN186955	JN186996	JN186819
Aethotaxis mitopteryx	Nototheniidae	YFTC 7768	JN186895	AY520106	JN186862	JN187038	JN186956	JN186997	JN186820
Dissostichus eleginoides	Nototheniidae	YFTC 3929	JN186896	JN186927	JN186863	JN187039	JN186957	JN186998	JN186821
Dissostichus mawsoni	Nototheniidae	YFTC 1226	AY256561	AY520110	AY517753	JN187040	JN186958	JN186999	JN186822

Gobionotothen acuta	Nototheniidae	YFTC 2339	JN186897	JN186928	JN186864	JN187041	JN186959	JN187000	JN186823
Gobionotothen gibberifrons	Nototheniidae	YFTC 1745	JN186898	AY520112	JN186865	JN187042	JN186960	JN187001	JN186824
Gobionotothen marionensis	Nototheniidae	YFTC 3662	JN186899	JN186929	JN186866	JN187043	JN186961	JN187002	JN186825
Lepidonotothen larseni	Nototheniidae	YFTC 1704	JN186900	AY520113	JN186867	JN187044	JN186962	JN187003	JN186826
Lepidonotothen nudifrons	Nototheniidae	YFTC 2020	JN186901	AY520114	JN186868	HM166362	HM166237	HM166212	HM166187
Lepidonotothen squamifrons	Nototheniidae	YFTC 2027	JN186902	AY520115	JN186869	JN187045	JN186963	JN187004	JN186827
Notothenia angustata	Nototheniidae	YFTC 1407	AY256562	AY520117	JN186870	JN187046	JN186964	JN187005	JN186828
Notothenia coriiceps	Nototheniidae	YFTC 2029	FJ647714	FJ647716	FJ647673	JN187047	JN186965	JN187006	JN186829
Notothenia rossii	Nototheniidae	YFTC 2031	AY256567	JN186930	JN186871	JN187048	JN186966	JN187007	JN186830
Patagonotothen cornucola	Nototheniidae	YFTC 6893	JN186903	N/A	JN186872	JN187049	JN186967	JN187008	JN186831
Patagonotothen elegans	Nototheniidae	YFTC 3947	JN186904	JN186931	JN186873	JN187050	JN186968	JN187009	JN186832
Patagonotothen guntheri	Nototheniidae	YFTC 3949	JN186905	JN186932	JN186874	JN187051	JN186969	JN187010	JN186833
Patagonotothen longipes	Nototheniidae	YFTC 6904	JN186906	N/A	JN186875	JN187052	JN186970	JN187011	JN186834
Patagonotothen ramsayi	Nototheniidae	YFTC 3998	JN186907	JN186933	JN186876	JN187053	JN186971	JN187012	JN186835

Patagonotothen sima	Nototheniidae	YFTC 6901	JN186908	N/A	JN186877	JN187054	JN186972	JN187013	JN186836
Patagonotothen tessellata	Nototheniidae	YFTC 4000	JN186909	JN186934	JN186878	HM166363	HM166238	HM166213	HM166188
Patagonotothen squamiceps	Nototheniidae	YFTC 7165	JN186910	JN186935	JN186879	JN187055	JN186973	JN187014	JN186837
Patagonotothen wiltoni	Nototheniidae	YFTC 7164	JN186911	N/A	JN186880	JN187056	JN186974	JN187015	JN186838
Pleuragramma antarcticum	Nototheniidae	YFTC 2034	JN186912	AY520108	N/A	JN187057	JN186975	JN187016	JN186839
Trematomus borchrevinki	Nototheniidae	YFTC 1393	FJ647716	AY520125	FJ647674	HM166364	HM166239	HM166214	HM166189
Trematomus bernacchii	Nototheniidae	YFTC 1401	AY256569	AY520126	FJ647676	HM166366	HM166241	HM166216	HM166191
Trematomus eulepidotus	Nototheniidae	YFTC 1799	FJ647718	FJ647642	FJ647680	HM166368	HM166243	HM166218	HM166193
Trematomus hansoni	Nototheniidae	YFTC 4225	FJ647748	FJ647646	FJ647684	JN187058	JN186976	JN187017	JN186840
Trematomus lepidorhinus	Nototheniidae	YFTC 13947	JN186913	JN186936	JN186871	HM166373	HM166248	HM166223	HM166198
Trematomus loennbergii	Nototheniidae	YFTC 2037	FJ647725	AY520127	FJ647689	HM166375	HM166250	HM166225	HM166200
Trematomus newnesi	Nototheniidae	YFTC 2040	FJ647729	FJ647653	FJ647693	HM166377	HM166252	HM166227	HM166202
Trematomus nicolai	Nototheniidae	YFTC 7735	FJ647731	FJ647656	FJ647696	HM166378	HM166253	HM166228	HM166203
Trematomus pennellii	Nototheniidae	YFTC 7807	FJ647742	FJ647660	FJ647700	JN187059	JN186977	JN187018	JN186841

Trematomus scotti	Nototheniidae	YFTC 2035	FJ647733	FJ647668	FJ647708	HM166383	HM166258	HM166233	HM166208
Trematomus tokarevi	Nototheniidae	YFTC 2340	FJ647739	FJ647669	FJ647710	HM166384	HM166259	HM166234	HM166209
Trematomus vicarius	Nototheniidae	YFTC 7166	FJ647741	FJ647671	FJ647712	HM166386	HM166261	HM166236	HM166211

Table S2. Relaxed-Clock Posterior Age Estimates in Millions of Years (Mya) for Most Recent Common Ancestors of Select Notothenioid Clades.

Clade	Mean Age (Mya)	95% Highest Posterior Density Interval (Mya)
Notothenioidei	77.9	63.8, 91.7
Bovichtidae	39.5	27.3, 55.3
Pseudaphritis urvillii and all other notothenioids	63.2	52.0, 75.5
Eleginops maclovinus and all other notothenioids	42.4	34.6, 50.6
Antarctic clade	22.4	19.7, 25.1
Pleuragrammatinae	17.0	12.5, 22.2
Dissostichus	7.3	3.9, 10.9
Harpagifer and Artedidraconidae	8.9	6.2, 11.5
Artedidraconidae	3.0	2.1, 3.9
Pogonophryne	1.1	0.7, 1.6
Cygnodraconinae	8.4	6.2, 10.6

Bathydraconinae	5.9	4.3, 7.6
Gymnodraconidae	6.0	3.9, 8.4
Channichthyidae	6.3	4.8, 7.8
Trematomus	9.1	6.7, 11.5
Patagonotothen	4.8	3.5, 6.1

Table S3. Effects of Extinction and Taxon Sampling Bias in Monte Carlo Constant Rates Tests.

Clade	γ-Statistic	Proportion Bias /Number of Missing Species	*p*-Values Calculated Over the Confidence Interval of λ_G and μ_G Estimates		
			Lower μ_G =0.81 λ_G=0.021	Median μ_G =0.87 λ_G=0.029	Upper μ_G =0.91 λ_G=0.039
Trematomus	-1.55	0.1 / 1	0.0016	0.0016	0.0010
Trematomus	-1.55	0.4 / 1	0.0018	0.0018	0.0020
Trematomus	-1.55	0.6 / 1	0.0015	0.0025	0.0026
Channichthyidae	-2.26	0.1 / 1	0.0002	0.0002	0.0002
Channichthyidae	-2.26	0.4 / 1	0.0002	0.0002	0.0002
Channichthyidae	-2.26	0.6 / 1	0.0002	0.0002	0.0002
Artedidraconidae	-1.75	0.1 / 1	0.0008	0.0008	0.0014
Artedidraconidae	-1.75	0.4 / 1	0.0008	0.0010	0.0014
Artedidraconidae	-1.75	0.6 / 1	0.0020	0.0020	0.0020

Table S4. Presence or Absence of Anti-Freeze Glycoproteins in Notothenioid Species.

Species	Family	AFGP	Method of Detection
Bovichtus variegatus	Bovichtidae	Absent	Southern blot
Pseudaphritis urvillii	Pseudaphritidae	Absent	Southern blot
Eleginops maclovinus	Eleginopidae	Absent	Southern blot
Dolloidraco longedorsalis	Artedidraconidae	Present	Protein isolation
Pogonophryne barsukovi	Artedidraconidae	Present	Protein isolation
Pogonophryne macropogon	Artedidraconidae	Present	Protein isolation
Pogonophryne marmorata	Artedidraconidae	Present	Protein isolation
Pogonophryne scotti	Artedidraconidae	Present	Protein isolation, Southern blot
Akarotaxis nudiceps	Bathydraconidae	Present	Protein isolation, Southern blot
Bathydraco macrolepis	Bathydraconidae	Present	Protein isolation
Bathydraco marri	Bathydraconidae	Present	Protein isolation
Bathydraco antarcticus	Bathydraconidae	Present	Protein isolation
Cygnodraco mawsoni	Bathydraconidae	Present	Protein isolation
Gerlachea australis	Bathydraconidae	Present	Protein isolation
Gymnodraco acuticeps	Bathydraconidae	Present	Freezing point assay
Racovitzia glacialis	Bathydraconidae	Present	Protein isolation
Chaenocephalus aceratus	Channichthyidae	Present	Freezing point assay
Chaenodraco wilsoni	Channichthyidae	Present	Protein isolation

Champsocephalus esox	Channichthyidae	Present	Southern blot
Chionodraco hamatus	Channichthyidae	Present	Protein isolation
Chionodraco myersi	Channichthyidae	Present	Protein isolation
Cryodraco antarcticus	Channichthyidae	Present	Protein isolation
Dacodraco hunteri	Channichthyidae	Present	Protein isolation
Neopagetopsis ionah	Channichthyidae	Present	Protein isolation
Pagetopsis macropterus	Channichthyidae	Present	Protein isolation, Southern blot
Pagetopsis maculatus	Channichthyidae	Present	Protein isolation
Harpagifer antarcticus	Harpagiferidae	Present	Southern blot
Aethotaxis mitopteryx	Nototheniidae	Present	Protein isolation
Dissostichus eleginoides	Nototheniidae	Present	Southern blot
Dissostichus mawsoni	Nototheniidae	Present	Protein isolation, Southern blot
Gobionotothen gibberifrons	Nototheniidae	Present	Freezing point assay, Protein isolation
Lepidonotothen squamifrons	Nototheniidae	Present	Protein isolation, Southern blot
Notothenia angustata	Nototheniidae	Present	Southern blot
Notothenia coriiceps	Nototheniidae	Present	Freezing point assay, Southern blot
Patagonotothen guntheri	Nototheniidae	Absent	Southern blot
Patagonotothen ramsayi	Nototheniidae	Absent	Southern blot
Patagonotothen tessellata	Nototheniidae	Absent	Southern blot

Pleuragramma antarcticum	Nototheniidae	Present	Protein isolation
Trematomus borchgrevinki	Nototheniidae	Present	Freezing point assay, Southern blot
Trematomus bernacchii	Nototheniidae	Present	Freezing point assay, Protein isolation
Trematomus eulepidotus	Nototheniidae	Present	Protein isolation
Trematomus hansoni	Nototheniidae	Present	Freezing point assay
Trematomus lepidorhinus	Nototheniidae	Present	Protein isolation
Trematomus loennbergii	Nototheniidae	Present	Freezing point assay, Protein isolation
Trematomus newnesi	Nototheniidae	Present	Southern blot
Trematomus nicolai	Nototheniidae	Present	Southern blot
Trematomus pennellii	Nototheniidae	Present	Protein isolation, Southern blot

Table S5. Buoyancy (%B) in Notothenioid Species.

Species	Family	Mean %B	Standard Deviation	Number of Specimens Measured
Bovichtus variegatus	Bovichtidae	5.87	0.41	6
Bovichtus diacanthus	Bovichtidae	5.02	0.03	4
Cottoperca gobio	Bovichtidae	4.58	0.20	11
Eleginops maclovinus	Eleginopidae	3.64	0.28	12
Dolloidraco longedorsalis	Artedidraconidae	4.49	0.78	17
Artedidraco skottsbergi	Artedidraconidae	5.40	1.05	7
Pogonophryne barsukovi	Artedidraconidae	3.44	0.68	35
Pogonophryne macropogon	Artedidraconidae	3.20	NA	2
Pogonophryne marmorata	Artedidraconidae	3.81	0.21	5
Pogonophryne scotti	Artedidraconidae	3.80	0.40	39
Akarotaxis nudiceps	Bathydraconidae	3.84	1.03	12
Bathydraco macrolepis	Bathydraconidae	4.38	0.48	5
Bathydraco marri	Bathydraconidae	4.37	0.79	7
Gerlachea australis	Bathydraconidae	3.29	0.46	4
Gymnodraco acuticeps	Bathydraconidae	3.38	0.31	39
Parachaenichthys charcoti	Bathydraconidae	4.39	0.59	39
Prionodraco evansii	Bathydraconidae	4.21	0.45	15
Racovitzia glacialis	Bathydraconidae	4.08	0.56	10
Vomeridens infuscipinnis	Bathydraconidae	1.57	0.27	7

Chaenocephalus aceratus	Channichthyidae	3.19	0.52	36
Chaenodraco wilsoni	Channichthyidae	3.08	0.31	28
Champsocephalus gunnari	Channichthyidae	2.90	0.23	46
Chionobathyscus dewitti	Channichthyidae	1.22	0.23	3
Chionodraco myersi	Channichthyidae	3.25	0.54	5
Chionodraco rastrospinosus	Channichthyidae	2.72	0.31	32
Cryodraco antarcticus	Channichthyidae	2.53	0.45	41
Dacodraco hunteri	Channichthyidae	1.41	0.37	5
Neopagetopsis ionah	Channichthyidae	1.28	0.17	33
Pagetopsis macropterus	Channichthyidae	2.38	0.24	27
Pagetopsis maculatus	Channichthyidae	3.11	NA	1
Pseudochaenichthys georgianus	Channichthyidae	1.96	0.28	30
Harpagifer antarcticus	Harpagiferidae	5.99	0.73	21
Aethotaxis mitopteryx	Nototheniidae	0	0	42
Dissostichus mawsoni	Nototheniidae	0	0	18
Gobionotothen gibberifrons	Nototheniidae	4.27	0.54	40
Lepidonotothen larseni	Nototheniidae	4.22	0.76	45
Lepidonotothen nudifrons	Nototheniidae	4.46	0.76	49
Lepidonotothen squamifrons	Nototheniidae	3.20	0.40	35
Notothenia angustata	Nototheniidae	4.43	0.39	8
Notothenia coriiceps	Nototheniidae	3.67	0.27	32
Notothenia rossii	Nototheniidae	3.55	0.65	20

Patagonotothen ramsayi	Nototheniidae	3.38	0.76	12
Patagonotothen tessellata	Nototheniidae	4.33	0.70	63
Pleuragramma antarcticum	Nototheniidae	0.34	0.50	91
Trematomus borchgrevinki	Nototheniidae	2.75	0.40	26
Trematomus bernacchii	Nototheniidae	3.52	0.42	49
Trematomus eulepidotus	Nototheniidae	3.41	0.51	30
Trematomus hansoni	Nototheniidae	3.12	0.40	52
Trematomus loennbergii	Nototheniidae	1.99	0.53	26
Trematomus newnesi	Nototheniidae	3.76	0.51	30
Trematomus nicolai	Nototheniidae	3.20	0.34	30
Trematomus pennellii	Nototheniidae	3.09	0.46	40
Trematomus scotti	Nototheniidae	4.14	0.32	12
Trematomus tokarevi	Nototheniidae	2.77	0.64	20